



Heterogeneous Li-alloy interphase enabling Li compensation during cycling for high energy density batteries

Xiancheng Wang^{a,1}, Chunhao Li^{a,1}, Yang Hu^b, Zihe Chen^a, Shuibin Tu^a, Jindi Wang^a, Zhao Cai^a, Hui Yang^c, Yongming Sun^{a,*}

^a Wuhan National Laboratory for Optoelectronics, Huazhong University of Science and Technology, Wuhan 430074, China

^b School of Optical and Electronic information, Huazhong University of Science and Technology, Wuhan 430074, China

^c Department of Mechanics, School of Aerospace Engineering, Huazhong University of Science and Technology, Wuhan 430074, China

ARTICLE INFO

Keywords:

Sn foil
Heterogeneous Li alloy interface
Uniform electrochemical reactions
Li compensation

ABSTRACT

Alloying elemental foil (e.g., Sn, Al, In, etc) anodes shows great promise for high-energy-density lithium (Li)-ion batteries due to their attractive capacities, low cost, and easy processability. The abundant Li loss, uneven electrochemical reactions, and continuous side reactions on cycling cause poor electrochemical performance. Herein, using Sn foil as a model system, we constructed a conformal heterogeneous Li-alloy interface alloying elemental foil (defined as “Sn/Li-LA”) with slightly higher delithiation potential than Li-Sn alloy. It could separate the electrolyte and active Li-Sn to suppress the side reactions between them, and meanwhile function as Li⁺ conductive layer to homogenize electrochemical reactions. Specially, an overpotential triggered Li compensation by Li-LA could extend the cycle life of batteries. As a result, the initial Coulombic efficiency of the Sn/Li-LA increased from 45.9% to 107.4%, and the average Coulombic efficiency increased from 98.6% to 99.5% for 350 cycles compared with the pristine Sn foil at 1 mA cm⁻² and 1 mAh cm⁻² in half cells, respectively. Full cells paired with LiNi_{0.6}Co_{0.2}Mn_{0.2}O (~15.3 mg cm⁻²) delivered high reversible capacities (~180 mAh g⁻¹, ~2.8 mAh cm⁻²) with stable cycling for 230 cycles in sharp contrast to the pristine Sn anode (~90 mAh g⁻¹, 1.4 mAh cm⁻²). In situ construction of Li-LA interface with donable active Li provides an effective approach to address the Li loss and extend the lifespan of high-capacity anode for advanced Li-based batteries.

1. Introduction

The pursuit of high-energy-density Li-ion batteries inspires the innovation of the advanced anode materials with high specific capacity, good cycling stability, and industry compatibility [1–4]. Alloying elemental foil (e.g., Sn, Al, In, etc) anode shows great promise for their attractive capacity (e.g., 990 mAh g⁻¹ and 1990.6 mAh cm⁻³ for Sn foil based on the full alloy reaction from Sn to Li₂₂Sn₅), low cost, and facile processability [5–8]. However, the application of alloying elemental foil anode is significantly restricted by several severe challenges, including side reactions at the electrode/electrolyte interphase, uneven electrochemical lithiation/delithiation reactions, and electro-mechanical instability [9,10]. The above issues lead to abundant active Li loss for the initial cycle and continuous capacity decay on cycling of pristine alloying elemental foil electrode, accompanied with failure of electrode structure and increases in resistance (Fig. 1a), showing low Coulombic

efficiency both for the initial cycle (e.g., Sn with initial Coulombic efficiency even below 50%) and on cycling (e.g., Sn with Coulombic efficiency < 99% during cycling) [11,12]. Studies have been continuously conducted to compensate the Li loss and improve electrochemical cycling of alloying elemental foil anode, which increase the reversible Li-ion capacity of full batteries (Fig. 1a, using Sn as a model system, noted as prelithiated Sn) [13–15]. The prelithiation could also enhanced the cycling stability of Sn foil electrode since the pre-expanded electrode could alleviate the subsequent strain/stress during cycling. However, the cycling life of the reported prelithiated Sn foil electrode is still far from the demand for practical battery applications due to the side reactions at the electrode/electrolyte interphase and inhomogeneity of electrochemical lithiation/delithiation reactions. Thus, it is highly expected to explore facile approach that can hinder undesirable side reactions, realize good homogeneity of the electrochemical reactions, and compensate Li loss when needed during cycling, which is of vital

* Corresponding author.

E-mail address: yongmingsun@hust.edu.cn (Y. Sun).

¹ These authors contributed equally to this work.

importance for a practical available alloying elemental foil anode for rechargeable high-energy-density batteries.

Herein, using Sn metal foil as a model system, we introduced a heterogeneous Li alloy interface on alloying elemental foil anode via mild chemical reaction between liquid alloy (Ga-In-Sn alloy) and metallic Li (defined as “Sn/Li-LA”). Due to “liquid” nature of liquid alloy and its good mechanical interaction with Sn foil, uniform prelithiation was realized without the need of large external pressure [16–18]. The Li-LA interphase could separate the electrolyte and active Sn, suppress the side reactions between them, and homogenize the electrochemical reactions, and thus enhancing the cycling stability [18,19]. It is noted that the delithiation potential of the Li-LA is slightly higher than the active Li-Sn alloy ($\Delta V = \sim 0.1$ V, Fig. 1b). Thus, Li compensation could take place once the increase of overpotential of full batteries trigger the delithiation of the Li-LA layer after long-term cycling, which prolong the lifespan of batteries (Fig. 1c). The Sn/Li-LA electrode delivered high initial Coulombic efficiency to 107.4% and high average Coulombic efficiency up to 99.5% for 350 cycles, benefited from the Li contribution and electro-mechanical stability arising from the Li-LA interphase. Paired with $\text{LiNi}_{0.6}\text{Co}_{0.2}\text{Mn}_{0.2}\text{O}$ (NCM622, mass loading of ~ 15.3 mg cm^{-2}), the NCM622||Sn/Li-LA cell delivered 45.4% increase in initial Coulombic efficiency and ~ 133.2 mAh g^{-1} increase in the reversible specific capacity after 230 cycles in comparison to the counterpart with pristine Sn electrode. Besides, the Sn/Li-LA electrode showed good ambient stability and achieved comparable electrochemical performance with fresh Sn/Li-LA electrode after exposure in air with high relative humidity of 81% for 24 hours. The introduction of heterogeneous Li-alloy interface on alloying elemental foil open new sight for functional prelithiation, which simultaneously considers the good electro-mechanical stability, ambient stability and the overpotential triggered Li compensation on cycling, showing great promise for the practical application of alloying elemental foil anode.

2. Experimental

2.1. Materials preparation

100 μm -thick Sn-based foil, consisting of 95wt% Sn and 5wt% Sb (denoted as Sn foil for simplicity), was received for direct use without further treatment. The Si electrode with active material mass loading of ~ 0.7 mg cm^{-2} was fabricated through a slurry process with 80wt% Si

particles, 10wt% carbon black and 10wt% Li polyacrylate acid binder. To fabricate Sn/Li-LA foil, Ga-In-Sn liquid alloy with Ga, In, Sn weight ratio of 68.5: 21.5: 10 was uniformly coated on Sn foil in ambient condition, and a metallic Li foil was stacked on the liquid alloy layer and heated at 60 $^{\circ}\text{C}$ for 12 hours in an argon filled glove box. Si/Li-LA and Cu/Li-LA electrodes was prepared using the same operations expect the replacement of Sn foil substrate by Si electrode and Cu foil, respectively.

2.2. Materials characterization

The morphology and structures of the Sn and Sn/Li-LA electrodes before and after cycling were conducted by SEM (Nova NanoSEM 450). The compositions and chemical states of the electrodes were detected by X-ray photoelectron spectroscopy (XPS, AXIS-ULTRA DLD-600W). The phases of the electrodes were identified by X-ray diffraction (XRD, Empyrean) with $\text{Cu-K}\alpha 1$ radiation under the accelerating voltage of 40 kV and current of 40 mA. The element composition and distribution were identified by EPMA (8050G).

2.3. Electrochemical evaluation

The electrochemical performances of Sn and Sn/Li-LA electrodes were evaluated in coin-type cells. The electrolyte was 1 M LiPF_6 in ethylene carbonate (EC)/dimethyl carbonate (DEC) (1: 1 in volume) with 5wt% fluoroethylene carbonate (FEC) and 1wt% vinyl carbonate (VC), unless otherwise stated. cyclic voltammetry (CV) for full cells was conducted at the voltage range between 3.7 V to 1.8 V (vs. Li/Li^+) with the scanning rate of 0.1 mV s^{-1} . Electrochemical impedance spectra (EIS) for half cells before and after cycling were collected at the frequency range from 100 mHz to 100 kHz. The equipment for the CV and EIS tests was VMP3 multichannel electrochemical workstation (Bio-Logic). The electrochemical cycling of Sn/Li-LA||Li and Sn||Li cells were performed by discharging at 1 mA cm^{-2} for 1 hour and then charging to 2 V (vs. Li/Li^+) for each cycle. $\text{LiNi}_{0.6}\text{Co}_{0.2}\text{Mn}_{0.2}\text{O}_2$ (NCM622) electrode with active mass loading of ~ 15.3 mg cm^{-2} was received from battery industry for direct use. The working potential for NCM622||Sn/Li-LA and NCM622||Sn full cells were 3.7 V to 1.8 V (vs. Li/Li^+). The full cells were first tested at 0.1 C ($1\text{ C} = 175$ mA g^{-1}) for activation and then cycled at 0.2 C subsequently. The mentioned dual-salt electrolyte was 0.6 M LiBF_4 and 0.6 M lithium difluoro(oxalato)borate (LiDFOB) in DEC/FEC (2: 1 in volume ratio).

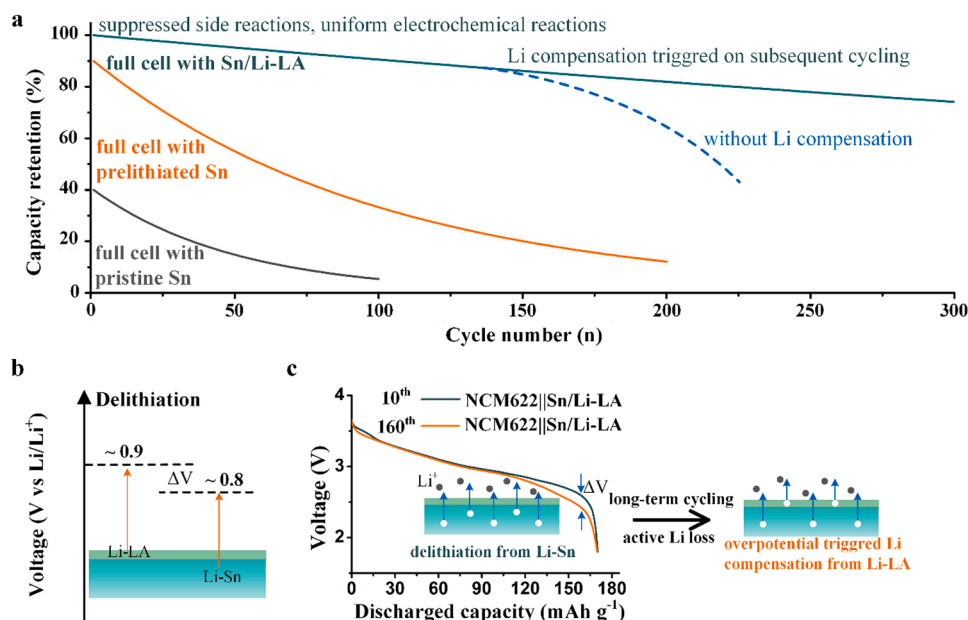


Fig. 1. (a) Schematic of the capacity retention-cycling number curves of full cells paired with pristine Sn foil, prelithiated Sn foil and Sn/Li-LA foil. The Li-LA interface on Sn foil could compensate the active Li loss on cycling, suppress side reactions between the active material and electrolyte, and homogenize electrochemical reactions. Thus the cells paired with Sn/Li-LA delivered high capacity and long cycling lifespan. (b) Design principle of heterogeneous Li-alloy interphase. Delithiation voltage of the Li-LA should be slightly higher than the active Li-Sn alloy. (c) The comparison of voltage-capacity curves of the NCM622||Sn/Li-LA at the 10th and 160th cycles. The insets showed Li compensation from Li-LA would be triggered once the overpotential after long-term cycling increased to ΔV in full cells.

2.4. Result and discussion

The fabrication of the Sn/Li-LA foil was schematically illustrated in Fig. 2a. LA was coated on the surface of Sn foil following by stacking a Li foil on the top. Spontaneous chemical lithiation reaction between the LA and metallic Li foil takes place to produce a Li-LA alloy interphase on the surface of Sn foil, and Sn/Li-LA foil was obtained after peeling off the residual Li foil. Fig. 2b showed the photos of the pristine Sn and Sn/Li-LA foils. With a heterogeneous interphase layer, the Sn/Li-LA foil displays uniform and smooth surface, similar to the pristine Sn foil. The dense surface structure was then revealed by scanning electron microscope (SEM) investigations, indicating that the uniform chemical lithiation reactions of LA and the successful formation of Li-LA functional layer on the Sn foil (Fig. S1-2). The element distribution of the as-achieved Sn/Li-LA foil was further investigated by electron probe microanalysis (EPMA). Uniform distribution of Ga element was observed over the entire foil surface in the top-view SEM image of the Sn/Li-LA electrode, again suggesting the uniform surface structure of Li-LA layer on Sn foil (Fig. 2c). The cross-section elemental mapping revealed uniform Li-LA layer with thickness of $\sim 10 \mu\text{m}$ (Fig. 2d). Note that the Ga signal was further extended into Sn layer to produce inner three-dimensional (3D) interdigitated Li-LA and Sn interphase under pure Li-LA surface, which could be due to the preferential chemical alloy reactions at the grain boundaries of Sn foil [20,21]. The inner interdigitated Li-LA and Sn interphase could provide stable mechanical support for stabilizing the

electrode structure on cycling, and 3D Li-conductive Li-LA provided abundant Li^+ transport pathway, which is beneficial for improving rate capability of the electrode (Fig. S5). XPS measurement of the pristine Sn and Sn/Li-LA foils were conducted to show their surficial chemical states of elements (Fig. 2e). A broad peak centered at 55.24 eV arose in the high-resolution Li 1s spectrum corresponding to Li-Ga alloy in the Sn/Li-LA foil, confirming the successful construction of Li-LA interphase on Sn foil. The generation of Li-Ga alloy and the Li-LA interphase were also confirmed by XRD. Compared with pristine Sn foil, new diffraction peaks at the 2θ positions of $\sim 24.78^\circ$, 44.19° and 48.65° were observed for the Sn/Li-LA foil (Fig. 2f), which corresponded to the phase of LiGa alloy (JCPDS #09-0043) [17]. With such a Li-LA interphase, the wettability between electrode and electrolyte was significantly improved. Sn/Li-LA electrode delivered a contact angle close to 0° with the carbonate electrolyte in contrast to 38° for pristine Sn electrode (Fig. S6, 7), which, together with the good ionic conductivity of Li-LA, could homogenize Li^+ flux, promote its transport, and homogenize lithiation/delithiation of active materials below.

To investigate the effect of the Li-LA interphase on the electrochemical property of Sn foil electrode, the Nyquist plots of fresh Sn/Li-LA||Li and Sn||Li cells were investigated (Fig. 3a, b). Compared with the pristine Sn electrode, a new semicircle arose in the Nyquist plots of the Sn/Li-LA electrode, consist with the formation of the Li-LA interface on Sn foil [22,23]. The small value for the corresponding interface impedance ($\sim 185.9 \text{ ohms}$) supported fast ionic diffusion capability of

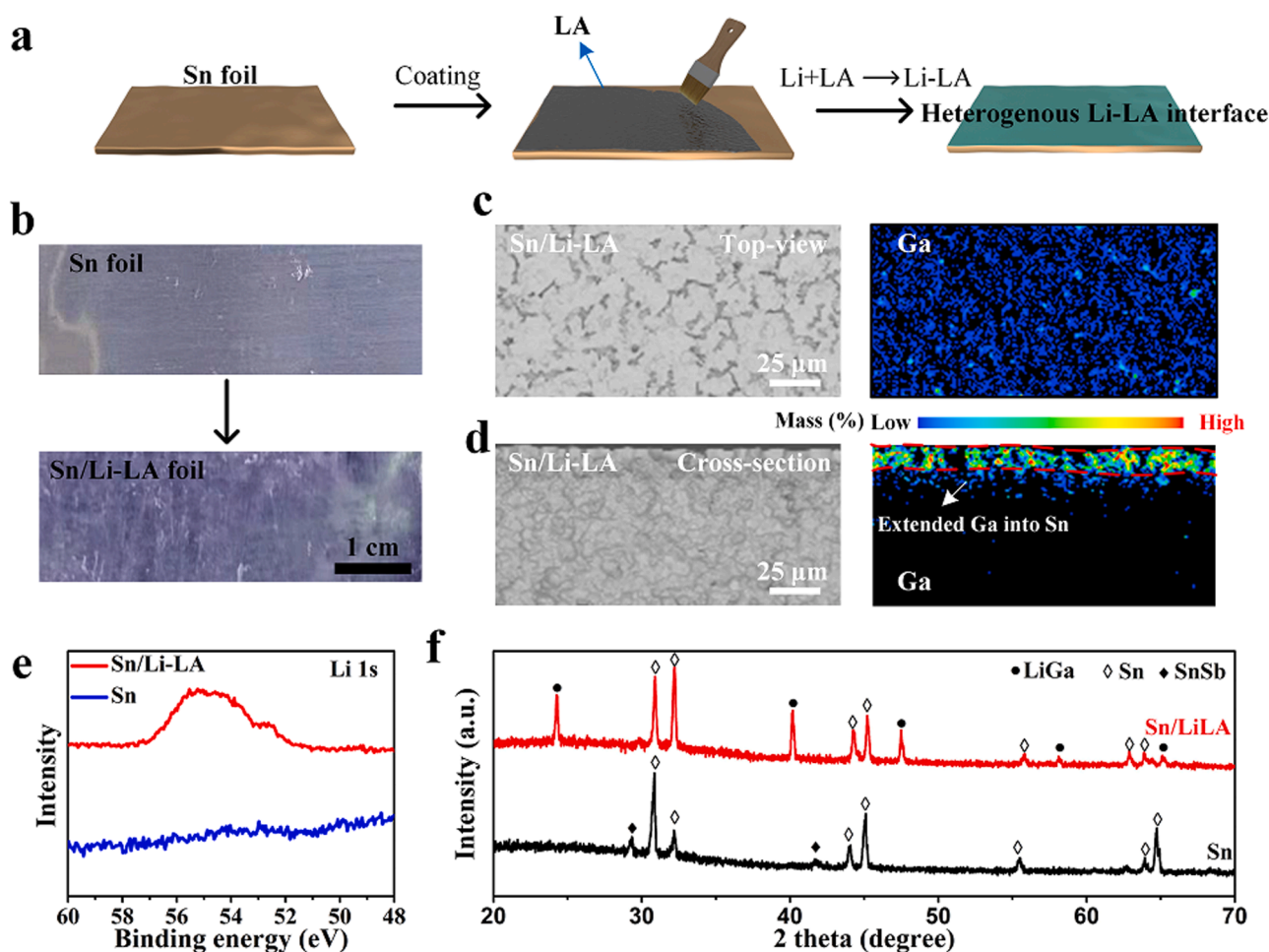


Fig. 2. (a) Schematic of the preparation processes of the Sn/Li-LA foil utilizing the chemical lithiation reaction between the metallic Li foil and LA coating layer. (b) Digital photos of the Sn and Sn/Li-LA foils. (c, d) Top-view and cross-section EPMA images and the corresponding Ga element mapping images of the Sn/Li-LA foil, respectively. (e) High-resolution Li 1s XPS results of the Sn/Li-LA and pristine Sn electrodes. (f) XRD patterns of the Sn (with 5wt% Sb doped) and the Sn/Li-LA foils (Sn: JCPDS#04-0673, SnSb: JCPDS#33-0118, and LiGa: JCPDS #09-0043).

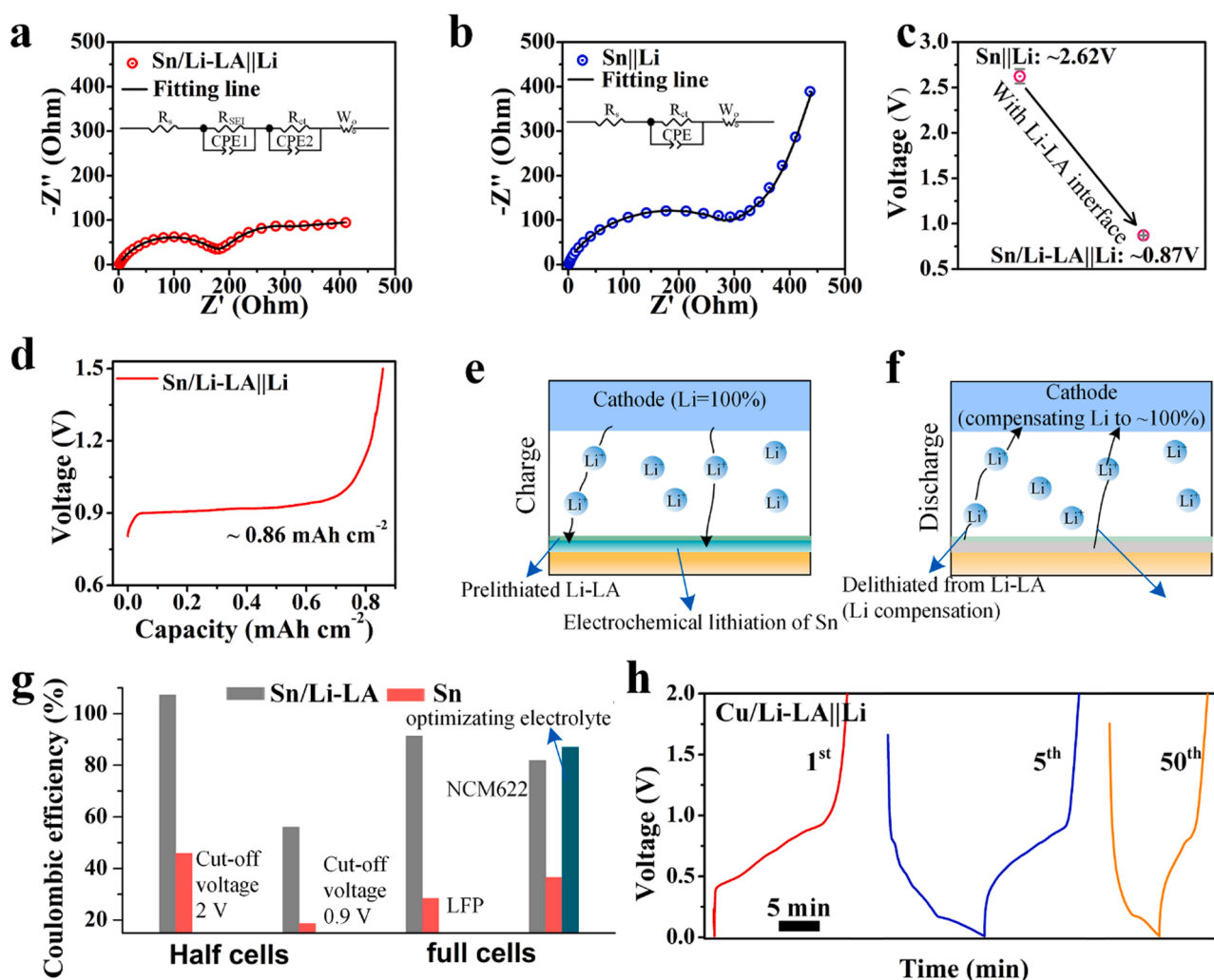


Fig. 3. (a, b) Nyquist plots of the Sn/Li-LA||Li and Sn||Li cells before cycling, respectively. The insets are the corresponding fitted equivalent circuit models [24]. (c) Open-circuit voltages of the Sn/Li-LA||Li and Sn||Li cells. (d) Delithiation capacity of the Sn/Li-LA foil by charging Sn/Li-LA||Li cell to 1.5 V (vs. Li/Li⁺) at the current density of 0.1 mA cm⁻². (e, f) Schematic of the electrochemical behavior of the Sn/Li-LA foil in full cell during the charge /discharge processes. (g) Comparisons of the initial Coulombic efficiency of Sn/Li-LA and Sn electrodes in half and full cells. (h) Charge/discharge curves of the Cu/Li-LA||Li cell for the 1st, 5th and 50th cycles. The test was conducted by discharge to 0.01 V followed by charging to 2 V (vs. Li/Li⁺) for each cycle.

such Li-LA layer. The impedance values for electron transport was reduced from ~ 379.3 to 217.9 ohms after introducing a Li-LA interphase. With the Li-LA interphase, the open-circuit potential (vs. Li/Li⁺) decreased from ~ 2.62 V for the pristine Sn electrode to ~ 0.87 V for the Sn/Li-LA electrode (Fig. 3c), which could effectively hinder the side reactions for gas formation on Sn foil anode and increase the initial Coulombic efficiency [11].

The initial charging curve of the Sn/Li-LA||Li cell showed a replenished Li⁺ capacity of ~ 0.86 mA cm⁻² with an average delithiation potential of ~ 0.9 V (vs. Li/Li⁺) (Fig. 3d), which was slightly higher than the Li-Sn alloy (~ 0.8 V for delithiation). Thus, the Li-LA could work as “Li donor” to prolong the cycle life once the overpotential of full cells increased on cycling. As schematically illustrated in Fig. 3e, f, Li⁺ was extracted from cathodes (e.g., NCM, LiFePO₄, etc) and came cross through the lithiated liquid alloy interface to lithiate the active Sn during the charge process. During the discharge process, Li⁺ went back to the cathode by dealloying of the active Li-Sn alloy. When active Li from the cathodes was inevitably consumed during the initial cycle and on cycling, Li-LA layer could act as “Li reservoir”, to donate active Li for compensation, and thus increase the reversible capacity and prolong the cycle life of batteries. The proposed working mechanism for Li compensation of Li-LA layer was further verified by electrochemical

charge/discharge measurement. By controlling the charge cut-off voltage of 2 V (vs. Li/Li⁺), the active Li in Li-LA would be fully extracted, and thus the Sn/Li-LA electrode showed a high initial Coulombic efficiency of 107.4%, outperforming to the pristine Sn electrode (45.9%, Fig. S9). When the cut-off voltage was reduced to 0.9 V (vs. Li/Li⁺) and the Sn/Li-LA electrode also delivered much higher initial Coulombic efficiency without the Li compensation effect from Li-LA than the pristine Sn electrode (37% higher, Fig. S10). The above results suggested the introduction of Li-LA interface for Li compensation to various anodes. We also extended this strategy to design a Si/Li-LA composite electrode with a high Coulombic efficiency of 113.6% (Fig. S11), showing good universality of the Li-LA interface for Li compensation to various anodes. The LiFePO₄||Sn/Li-LA cell delivered an initial Coulombic efficiency of 91.4%, much higher than 28.4% for the LiFePO₄||Sn cell, and the initial Coulombic efficiency was also increased from 36.6% for NCM622||Sn cell to 82.0% for NCM622||Sn/Li-LA, showing great potential for practical application (Fig. S12, 13). It should be noted that the initial Coulombic efficiency could be further improved by coupling electrolyte engineering. By replacing regular LiPF₆ based carbonate electrolyte (1 M LiPF₆ in EC/DEC (1: 1 in volume ratio) with 5wt% FEC and 1wt% VC) by dual-salt electrolyte (0.6 M LiBF₄ and 0.6 M LiDFOB in DEC/FEC (2: 1 in

volume ratio)), the initial Coulombic efficiency was increased from 82.0% to 87.1% for NCM622||Sn/Li-LA cell (Fig. S14). To further reveal the reversibility of Li-LA alloy in promoting the battery electrochemical cycling, Li-LA was constructed on Cu foil to form Cu/Li-LA electrode, which delivered a stable cycling for over 200 cycles (Fig. 3h, S15). The high reversibility of the lithiation/delithiation behavior of the Li-LA electrode supported that the stored active Li in Li-LA could be donated to compensate gradually Li consumption on cycling, and thus ensuring high capacity retention for long-term cycling.

Fig. 4a, b schematically illustrated the structural evolutions of the Sn/Li-LA and Sn electrodes, respectively. The Li^+ conductive Li-LA interface on the Sn foil enabled uniform lithiation/delithiation behavior on cycling, ensuring good electro-mechanical stability and cycling stability [25]. In contrast, uneven lithiation behavior occurred for the pristine Sn foil, which would cause serious local stress concentration and thus electrode crack and even pulverization on subsequent cycles. SEM was performed to investigate the electrode structures after cycling. Sn/Li-LA electrode displayed a uniform lithiation layer with thickness of $\sim 25 \mu\text{m}$ after initial intake of 3 mAh cm^{-2} Li (Fig. 4c), in sharp contrast to uneven lithiation behavior of the pristine Sn electrode with Li penetration depth range from ~ 30 to $45 \mu\text{m}$ in the observed area

(Fig. 4d). Good structural integrity of electrodes was maintained for the Sn/Li-LA electrode after 50th, 100th, and 250th cycles. Dense structure without cracks/pulverization was confirmed for the Sn/Li-LA electrode, due to the uniform lithiation reaction and good electro-mechanical stability enabled by the Li-LA interphase (Fig. 4e, g and h). An integrated electrode structure was evidenced without showing new interfacial layer between Sn and Li-LA, probing the good stability of the Sn/Li-LA electrode [26,27]. In comparison, the pristine Sn electrode experienced continuous structural evolution on cycling. After only 50 cycles (Fig. 4f), cracks with size of 30 to 46 μm were shown randomly in the electrode, which extended to 43 μm in depth over the thickness in the selected location. The situation got even deteriorated after prolonged cycles (100, 250 cycles, Fig. 4i, j, and S16), and cracks were aggravated with cycling, resulting in the peeling off of large pieces of active materials with size from 260 to 420 μm after 250 cycles. The large difference in the structures of the pristine Sn and Sn/Li-LA electrodes after cycling strongly suggested the advancement of Li-LA interphase in homogenizing the electrochemical reactions and improving the electro-mechanical stability of Sn foil anode.

The charge/discharge curves were further compared at different lithiation/delithiation cycles (Fig. 4k, l). For Sn/Li-LA electrode, the

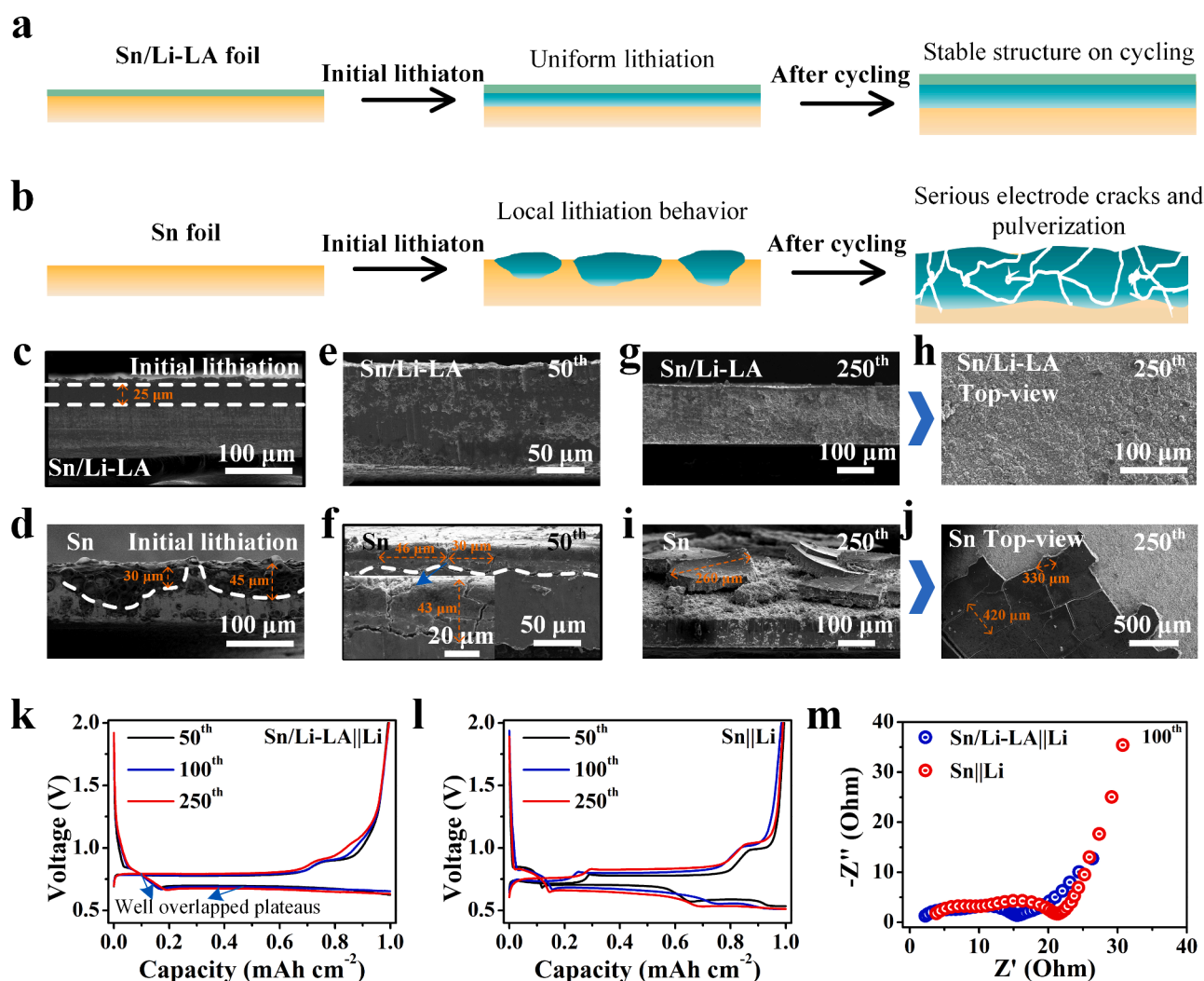


Fig. 4. (a, b) Schematic of the structural evolutions of the Sn/Li-LA and Sn electrodes over lithiation/delithiation cycling. (c, d) Cross-section SEM images of the Sn/Li-LA and Sn electrodes after the initial lithiation at 1 mA cm^{-2} for 3 hours, respectively. (e, f) Cross-section SEM images of the Sn/Li-LA and Sn electrodes after 50 cycles, respectively. (g, h) Cross-section SEM and top-view images of the Sn/Li-LA electrode after 250 cycles, respectively. (i, j) Cross-section SEM and top-view SEM images of the pristine Sn electrode after 250 cycles. (k, l) Voltage-capacity curves of the Sn/Li-LA and Sn electrodes at the 50th, 100th and 250th cycles, respectively. (m) Nyquist plots of the Sn/Li-LA||Li and Sn||Li cells after 100 cycles. The tests were conducted by discharging at 1 mA cm^{-2} for 1 hour followed by charging to 2 V (vs. Li/Li^+) at the same current density.

short lithiation voltage slope from 0.85 to 0.70 V (vs. Li/Li⁺) corresponded to the electrochemical formation of Sb to Li₃Sb, Ga to LiGa and Sn to Li₂Sn₅ [28,29]. The long lithiation voltage plateau with average voltage of 0.68 V (vs. Li/Li⁺) arose from the further lithiation of Li₂Sn₅ to LiSn phase. The curves of Sn/Li-LA were well overlapped on cycling with constant capacity ratio of 1/4, demonstrating the stable electrochemical performance of the Sn/Li-LA electrode. In contrast, pristine Sn electrode exhibited multi-voltage lithiation plateaus with average voltages of 0.85, 0.77, 0.70, 0.59 and 0.53 V (vs. Li/Li⁺), corresponding to the electrochemical alloy reactions from Sb to Li₃Sb, Sn to Li₂Sn₅, Li₂Sn₅ to LiSn, LiSn to Li₇Sn₃ and Li₇Sn₃ to Li₁₇Sn₅, respectively [30,31]. These voltage plateaus and the corresponding capacity contribution varied on

cycling, which suggested the inhomogeneous electrochemical reactions and unstable electrode structure. Such results agreed well with the observed structure evolution of electrodes (Fig. 4c to j). EIS measurement was also conducted to clarify the interface properties of the electrodes on cycling. The results showed that the introduction of the Li-LA interface stabilized the interface impedance to a low value, again supporting the outperforming stability of the Sn/Li-LA electrode (Fig. 4m, S17).

The potential of the practical implantation of the Sn/Li-LA in Li-ion batteries was further evaluated in both half and full cell configurations. The Sn/Li-LA electrode delivered stable cycling up to 350 lithiation/delithiation cycles and high average Coulombic efficiency of 99.5% in a

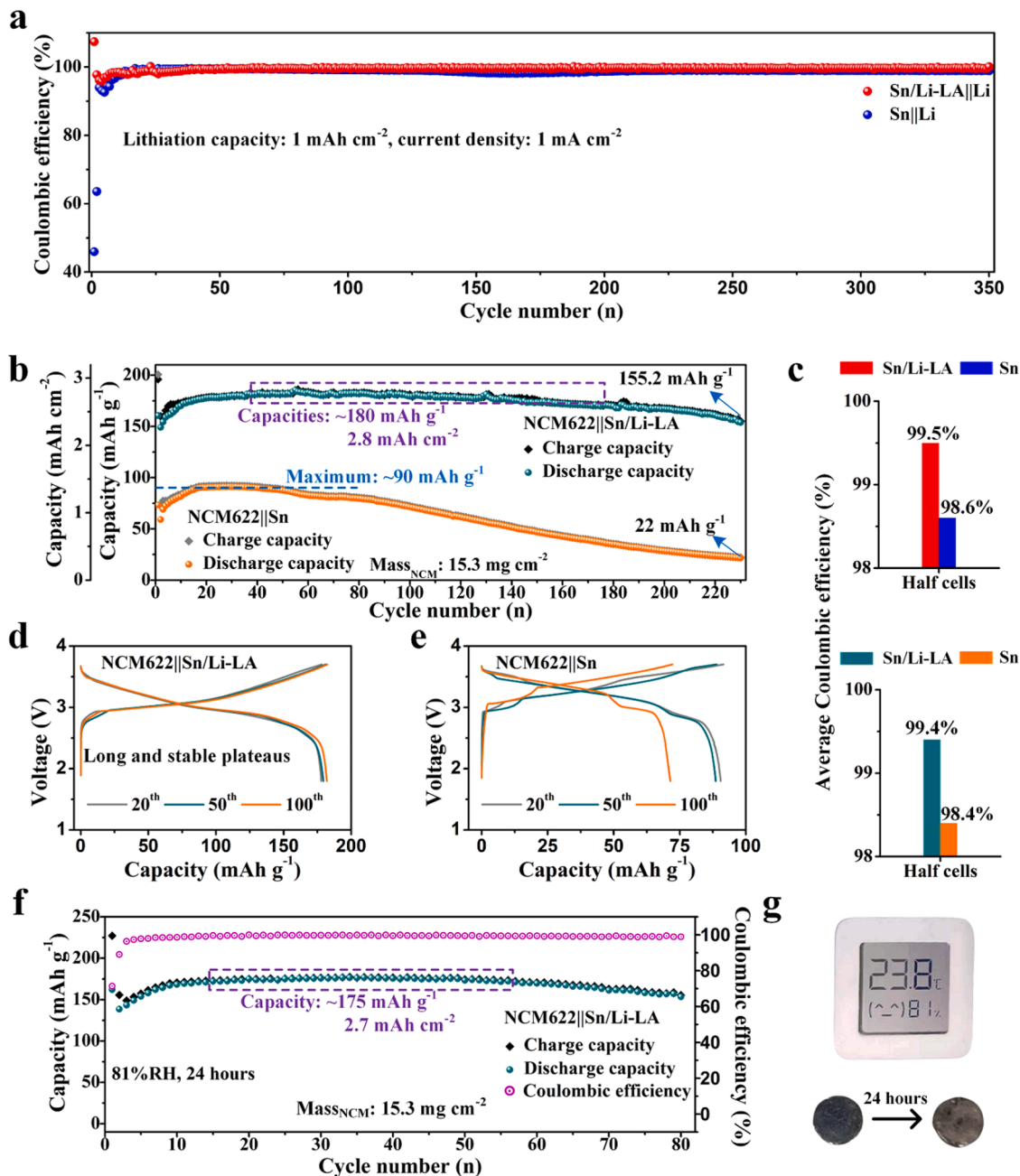


Fig. 5. (a) Coulombic efficiency-cycle number plots of the Sn/Li-LA||Li and Sn||Li cells. (b) Electrochemical performance of NCM622||Sn/Li-LA and NCM622||Sn cells. (c) Average Coulombic efficiency of the Sn/Li-LA and Sn electrodes in half cell corresponding to (a) and full cell corresponding to (b), respectively. (d, e) Charge/discharge curves of NCM622||Sn/Li-LA and NCM622||Sn cells at the 20th, 50th and 100th cycles. (f) Electrochemical cycling of NCM622||Sn/Li-LA full cell using dual-salt electrolyte. The Sn/Li-LA electrode was exposed in ambient condition with the relative humidity of 81% for 24 hours before use. (g) The digital photo of the temperature and humidity indicator to show the test conditions and the corresponding digital photos of the electrodes before and after exposure.

regular carbonate electrolyte at 1 mA cm⁻² and 1 mAh cm⁻², which was higher than 98.6% for the counterpart with Sn (Fig. 5a). It is noted that 1% increase for cycling Coulombic efficiency is a significant improvement, which means that the 1 mAh cm⁻² accumulated Li loss would be saved per 100 cycles at this test condition [32]. When paired with NCM622 cathode with a mass loading of ~15.3 mg cm⁻², the NCM622||Sn/Li-LA showed stable cycling with a high reversible specific capacity up to 180 mAh g⁻¹ (2.8 mAh cm⁻²) in average at 0.2 C, while the full cell with pristine Sn electrode displayed fast capacity decay and showed low cycled capacity below 100 mAh g⁻¹ (Fig. 5b, c). The low reversible capacity of the NCM622||Sn cell arose from the very low Coulombic efficiency of the pristine Sn foil. The continuous active Li loss caused the relatively low Coulombic efficiency and gradually capacity decay on cycling from 90 mAh g⁻¹ for the 20th cycle to 22 mAh g⁻¹ for the 230 cycles. The full cell with the Sn/Li-LA anode showed higher value of Coulombic efficiency at each cycle than the counterpart with the pristine Sn anode, indicating the enhanced electrochemical reversibility of the electrode with the Li-LA interface (Fig. S18) [33–35]. The results of CV (Fig. S19) and charge/discharge measurements (Fig. 5d, e) on cycling synthetically confirmed highly stable electrochemical reactions of NCM622||Sn/Li-LA cells. Moreover, the charge and discharge curves for 20th, 50th and 100th cycles were almost fully overlapped without showing increase in overpotential on cycling, indicating the stable lithiation/delithiation reactions of the Sn/Li-LA electrode. In sharp contrast, continuous change in voltage curves and capacities were observed for the NCM622||Sn cells. The stability of electrode in the air condition was critical for the practical applications [36,37]. Sn/Li-LA electrode was rested in the ambient condition with a high relative humidity of 81% for 24 hours before cell assembling. The NCM622||Sn/Li-LA delivered high reversible capacity (175 mAh g⁻¹, 2.7 mAh cm⁻²) and stable cycling (over 80 cycles), probing the good resistance to the high-humidity condition of the prelithiated Li-LA interface and the promise of Sn/Li-LA electrode for practical applications (Fig. 5f, g).

3. Conclusion

In summary, we successfully constructed a Li-LA interface on the Sn foil, which homogenized electrochemical lithiation behavior, stabilized electrode structure, reduced the side reactions, and provided donable Li-ion capacity. When applied to Li-ion batteries, the Sn/Li-LA electrode delivered high initial Coulombic efficiency and superior cyclic stability in both half and full cell configurations. NCM622||Sn/Li-LA cell with high cathode mass loading of ~15.3 mg cm⁻² delivered stable cycling for 230 cycles with a high reversible specific capacity up to 180 mAh g⁻¹ (2.8 mAh cm⁻²) and a high average Coulombic efficiency of 99.4% at 0.2 C. Meanwhile, the Sn/Li-LA electrode showed superior ambient stability in a high humidity environment, and thus potentially compatible with the battery industry. This research provided new sight into the Li compensation and improvement of the electro-mechanical stability of high-specific-capacity alloy-type anodes for the high energy density battery systems.

CRedit authorship contribution statement

Xiancheng Wang: Investigation, Data curation, Methodology, Writing – original draft. **Chunhao Li:** Data curation, Methodology. **Yang Hu:** Data curation, Methodology. **Zihe Chen:** Data curation. **Shuibin Tu:** Methodology. **Jindi Wang:** Investigation. **Zhao Cai:** Investigation. **Hui Yang:** Investigation. **Yongming Sun:** Supervision, Conceptualization, Methodology, Writing – review & editing.

Declaration of Competing Interest

The authors declare no competing financial interest.

Acknowledgements

The authors would like to thank the support by National Natural Science Foundation of China (No. 52072137, 52272207). Hui Yang would like to thank the support by National Natural Science Foundation of China (No. 12172143). The authors would like to thank the Analytical and Testing Center of Huazhong University of Science and Technology for conducting the materials characterization.

Supplementary materials

Supplementary material associated with this article can be found, in the online version, at doi:10.1016/j.ensm.2022.11.010.

References

- [1] M.N. Obrovac, V.L. Chevrier, Alloy negative electrodes for Li-ion batteries, *Chem. Rev.* 114 (2014) 11444–11502, <https://doi.org/10.1021/cr500207g>.
- [2] B.T. Heligman, K.J. Kreder, A. Manthiram, Zn-Sn interdigitated eutectic alloy anodes with high volumetric capacity for lithium-ion batteries, *Joule* 3 (2019) 1051–1063, <https://doi.org/10.1016/j.joule.2019.01.005>.
- [3] Steven T. Boles, M.H. Tahmasebi, Are foils the future of anodes? *Joule* 4 (2020) 1342–1346, <https://doi.org/10.1016/j.joule.2020.05.009>.
- [4] M. Li, J. Lu, Z. Chen, K. Amine, 30 years of lithium-ion batteries, *Adv. Mater.* 30 (2018), e1800561, <https://doi.org/10.1002/adma.201800561>.
- [5] H. Li, T. Yamaguchi, S. Matsumoto, H. Hoshikawa, T. Kumagai, N.L. Okamoto, T. Ichitsubo, Circumventing huge volume strain in alloy anodes of lithium batteries, *Nat. Commun.* 11 (2020) 1584, <https://doi.org/10.1038/s41467-020-15452-0>.
- [6] B.T. Heligman, A. Manthiram, Elemental foil anodes for lithium-ion batteries, *ACS Energy Lett* 6 (2021) 2666–2672, <https://doi.org/10.1021/acseenergylett.1c01145>.
- [7] G. Wang, M. Aubin, A. Mehta, H. Tian, J. Chang, A. Kushima, Y. Sohn, Y. Yang, Stabilization of Sn anode through structural reconstruction of a Cu-Sn intermetallic coating layer, *Adv. Mater.* 32 (2020), e2003684, <https://doi.org/10.1002/adma.202003684>.
- [8] B.-Q. Xiong, X. Zhou, G.-L. Xu, X. Liu, Y. Hu, Y. Liu, L. Zhu, C.-G. Shi, Y.-H. Hong, S.-C. Wan, C.-J. Sun, S. Chen, L. Huang, S.-G. Sun, K. Amine, F.-S. Ke, In situ construction of an ultrarobust and lithiophilic Li-enriched Li-N nanoshield for high-performance Ge-based anode materials, *ACS Energy Lett.* 5 (2020) 3490–3497, <https://doi.org/10.1021/acseenergylett.0c02121>.
- [9] R. Zhan, X. Wang, Z. Chen, Z.W. Seh, L. Wang, Y. Sun, Promises and challenges of the practical implementation of prelithiation in lithium-ion batteries, *Adv. Energy Mater.* 11 (2021), <https://doi.org/10.1002/aenm.202101565>.
- [10] K.J. Kreder, B.T. Heligman, A. Manthiram, Interdigitated eutectic alloy foil anodes for rechargeable batteries, *ACS Energy Lett.* 2 (2017) 2422–2423, <https://doi.org/10.1021/acseenergylett.7b00844>.
- [11] H. Xu, S. Li, C. Zhang, X. Chen, W. Liu, Y. Zheng, Y. Xie, Y. Huang, J. Li, Roll-to-roll prelithiation of Sn foil anode suppresses gassing and enables stable full-cell cycling of lithium ion batteries, *Energy Environ. Sci.* 12 (2019) 2991–3000, <https://doi.org/10.1039/c9ee01404g>.
- [12] H. Xu, S. Li, X. Chen, C. Zhang, W. Liu, H. Fan, Y. Yu, Y. Huang, J. Li, Sn-alloy foil electrode with mechanical prelithiation: Full-cell performance up to 200 cycles, *Adv. Energy Mater.* 9 (2019), <https://doi.org/10.1002/aenm.201902150>.
- [13] N. Liang, H. Xu, H. Fan, Z. Li, S. Li, Cryogenic mechanical prelithiation reduces porosity and improves battery performance of an alloy foil anode, *ACS Appl. Mater. Interfaces* 14 (2022) 13326–13334, <https://doi.org/10.1021/acsaami.1c24704>.
- [14] S. Li, C. Wang, J. Yu, Y. Han, Z. Lu, Understanding the role of conductive polymer in thermal lithiation and battery performance of Li-Sn alloy anode, *Energy Storage Mater.* 20 (2019) 7–13, <https://doi.org/10.1016/j.ensm.2018.11.030>.
- [15] J. Lou, K. Chen, N. Yang, Y. Shuai, C. Zhu, Improved cycle stability of LiSn alloy anode for different electrolyte systems in lithium battery, *Nanomaterials* 11 (2021) 1–8, <https://doi.org/10.3390/nano11020300>.
- [16] J. Meng, Y. Zhang, X. Zhou, M. Lei, C. Li, Li₂CO₃-affiliative mechanism for air-accessible interface engineering of garnet electrolyte via facile liquid metal painting, *Nat. Commun.* 11 (2020) 3716, <https://doi.org/10.1038/s41467-020-17493-x>.
- [17] D. Wang, Y. Liu, G. Li, C. Qin, L. Huang, Y. Wu, Liquid metal welding to suppress Li dendrite by equalized heat distribution, *Adv. Funct. Mater.* 31 (2021), 2106740, <https://doi.org/10.1002/adfm.202106740>.
- [18] C. Wei, L. Tan, Y. Tao, Y. An, Y. Tian, H. Jiang, J. Feng, Y. Qian, Interfacial passivation by room-temperature liquid metal enabling stable 5 V-class lithium-metal batteries in commercial carbonate-based electrolyte, *Energy Storage Mater.* 34 (2021) 12–21, <https://doi.org/10.1016/j.ensm.2020.09.006>.
- [19] B. Han, D. Xu, S.S. Chi, D. He, Z. Zhang, L. Du, M. Gu, C. Wang, H. Meng, K. Xu, Z. Zheng, Y. Deng, 500 Wh kg⁻¹ class Li metal battery enabled by a self-organized core-shell composite anode, *Adv. Mater.* 32 (2020), 2004793, <https://doi.org/10.1002/adma.202004793>.
- [20] Z. Cai, Y. Ou, B. Zhang, J. Wang, L. Fu, M. Wan, G. Li, W. Wang, L. Wang, J. Jiang, Z.W. Seh, E. Hu, X.Q. Yang, Y. Cui, Y. Sun, A replacement reaction enabled interdigitated metal/solid electrolyte architecture for battery cycling at 20 mA cm⁻²

- ²⁾ and 20 mAh cm⁻², *J. Am. Chem. Soc.* 143 (2021) 3143–3152, <https://doi.org/10.1021/jacs.0c11753>.
- [21] J.B. Park, C. Choi, S. Yu, K.Y. Chung, D.W. Kim, Porous lithiophilic Li–Si alloy-type interfacial framework via self-discharge mechanism for stable lithium metal anode with superior rate, *Adv. Energy Mater.* 11 (2021), <https://doi.org/10.1002/aenm.202101544>.
- [22] M. Gaberscek, Understanding Li-based battery materials via electrochemical impedance spectroscopy, *Nat. Commun.* 12 (2021) 6513, <https://doi.org/10.1038/s41467-021-26894-5>.
- [23] C. Yan, X.B. Cheng, Y.X. Yao, X. Shen, B.Q. Li, W.J. Li, R. Zhang, J.Q. Huang, H. Li, Q. Zhang, An armored mixed conductor interphase on a dendrite-free lithium-metal anode, *Adv. Mater.* 30 (2018), e1804461, <https://doi.org/10.1002/adma.201804461>.
- [24] S. Tu, X. Ai, X. Wang, S. Gui, Z. Cai, R. Zhan, Y. Tan, W. Liu, H. Yang, C. Li, Y. Sun, Circumventing chemo-mechanical failure of Sn foil battery anode by grain refinement and elaborate porosity design, *J. Energy Chem.* 62 (2021) 477–484, <https://doi.org/10.1016/j.jechem.2021.03.053>.
- [25] X. Jin, Z. Cai, X. Zhang, J. Yu, Q. He, Z. Lu, M. Dahbi, J. Alami, J. Lu, K. Amine, H. Zhang, Transferring liquid metal to form a hybrid solid electrolyte via a wettability-tuning technology for lithium-metal anodes, *Adv. Mater.* 34 (2022), e2200181, <https://doi.org/10.1002/adma.202200181>.
- [26] Z. Ju, G. Lu, O. Sheng, H. Yuan, S. Zhou, T. Liu, Y. Liu, Y. Wang, J. Nai, W. Zhang, X. Tao, Soybean protein fiber enabled controllable Li deposition and a LiF-nanocrystal-enriched interface for stable Li metal batteries, *Nano Lett.* 22 (2022) 1374–1381, <https://doi.org/10.1021/acs.nanolett.1c04775>.
- [27] O. Sheng, C. Jin, M. Chen, Z. Ju, Y. Liu, Y. Wang, J. Nai, T. Liu, W. Zhang, X. Tao, Platinum nano-interlayer enhanced interface for stable all-solid-state batteries observed via cryo-transmission electron microscopy, *J. Mater. Chem. A* 8 (2020) 13541–13547, <https://doi.org/10.1039/d0ta03270k>.
- [28] C. Huang, X. Wang, Q. Cao, D. Zhang, J.-Z. Jiang, A self-healing anode for Li-ion batteries by rational interface modification of room-temperature liquid metal, *ACS Appl. Energy Mater.* 4 (2021) 12224–12231, <https://doi.org/10.1021/acsaem.1c01951>.
- [29] X. Guo, Y. Ding, L. Xue, L. Zhang, C. Zhang, J.B. Goodenough, G. Yu, A self-healing room-temperature liquid-metal anode for alkali-ion batteries, *Adv. Funct. Mater.* (2018) 28, <https://doi.org/10.1002/adfm.201804649>.
- [30] H. Xu, S. Li, X. Chen, C. Zhang, Z. Tang, H. Fan, Y. Yu, W. Liu, N. Liang, Y. Huang, J. Li, Surpassing lithium metal rechargeable batteries with self-supporting Li–Sn–Sb foil anode, *Nano Energy* (2020) 74, <https://doi.org/10.1016/j.nanoen.2020.104815>.
- [31] Z. Yi, Z. Wang, Y. Cheng, L. Wang, Sn-based intermetallic compounds for Li-ion batteries: Structures, lithiation mechanism, and electrochemical performances, *Energy Environ. Mater.* 1 (2018) 132–147, <https://doi.org/10.1002/eem2.12016>.
- [32] C. Li, S. Tu, X. Ai, S. Gui, Z. Chen, W. Wang, X. Liu, Y. Tan, H. Yang, Y. Sun, Stress-Regulation design of lithium alloy electrode toward stable battery cycling, *Energy Environ. Mater.* 0 (2022) 1–8, <https://doi.org/10.1002/eem2.12267>.
- [33] L. Tan, C. Wei, Y. Zhang, S. Xiong, H. Li, J. Feng, Self-assembled, highly-lithiophilic and well-aligned biomass engineered MXene paper enables dendrite-free lithium metal anode in carbonate-based electrolyte, *J. Energy Chem.* 69 (2022) 221–230, <https://doi.org/10.1016/j.jechem.2022.01.024>.
- [34] C.Y. Fan, D. Xie, X.H. Zhang, W.Y. Diao, R. Jiang, X.L. Wu, Homogeneous Li⁺ flux distribution enables highly stable and temperature-tolerant lithium anode, *Adv. Funct. Mater.* 31 (2021), 2102158, <https://doi.org/10.1002/adfm.202102158>.
- [35] Z.-Y. Gu, J.-Z. Guo, Z.-H. Sun, X.-X. Zhao, X.-T. Wang, H.-J. Liang, X.-L. Wu, Y. Liu, Air/water/temperature-stable cathode for all-climate sodium-ion batteries, *Cell Rep. Phys. Sci.* 2 (2021), 100665, <https://doi.org/10.1016/j.xcrp.2021.100665>.
- [36] J. Zhao, Z. Lu, H. Wang, W. Liu, H.W. Lee, K. Yan, D. Zhuo, D. Lin, N. Liu, Y. Cui, Artificial solid electrolyte interphase-protected Li_xSi nanoparticles: An efficient and stable prelithiation reagent for lithium-ion batteries, *J. Am. Chem. Soc.* 137 (2015) 8372–8375, <https://doi.org/10.1021/jacs.5b04526>.
- [37] B. Huang, T. Huang, L. Wan, A. Yu, Pre-lithiating SiO anodes for lithium-ion batteries by a simple, effective, and controllable strategy using stabilized lithium metal powder, *ACS Sustain. Chem. Eng.* 9 (2021) 648–657, <https://doi.org/10.1021/acssuschemeng.0c05851>.